

MAGNETO-SENSITIVE CARBON-INORGANIC COMPOSITES BASED ON PARTICLEBOARD AND PLYWOOD WASTES

Mariia Galaburda¹*, Viktor Bogatyrov¹, Dariusz Sternik², Olena Oranska¹,
Mykola Borysenko¹, Ivan Škorvák³, Ewa Skwarek²,
Anna Deryło-Marczewska², Volodymyr Gun'ko¹

¹Chuiko Institute of Surface Chemistry, National Academy of Sciences of Ukraine,
17, General Naumov str., Kyiv 03164, Ukraine

²Faculty of Chemistry, Maria Curie-Skłodowska University, 3, Maria Curie-Skłodowska sq., Lublin 20031, Poland

³Institute of Experimental Physics, Slovak Academy of Sciences, 47, Watsonova str., Košice 04001, Slovak Republic
*e-mail: mariia.galaburda@gmail.com

Abstract. A study of conversion of metal-modified (Fe, Co) sawdust into magneto-sensitive porous composites using thermal carbonization process in an inert atmosphere is reported herein. Furniture wastes derived from particleboard and plywood were used as raw precursors. The as-prepared materials were characterized using nitrogen adsorption, X-ray diffraction, scanning electron microscopy and thermal analysis methods. The effects of metal precursors on the structure and morphology of metal-carbon nanocomposites as well on their magnetic properties were investigated. The results show that the structural and morphological characteristics of the obtained materials depend strongly on the metal precursor's types. The specific surface area of micro-mesoporous composites was $\approx 58, 328,$ and $391 \text{ m}^2/\text{g}$ for Fe/C, Co/C, and FeCo/C, respectively, at the total pore volume of ca. $0.2 \text{ cm}^3/\text{g}$. The efficiency of the composites in dyes sorption was studied. The unmodified sawdust carbon exhibited nonporous structure at $S_{BET} = 4 \text{ m}^2/\text{g}$ and very low adsorption capacity. The maximum adsorption capacity of the composites was in the range of 2.8-31 mg/g and depended strongly on the textural characteristics of adsorbents. All samples exhibited soft magnetic properties with the saturation magnetization of 6.6, 53, 13.5 Am²/kg for Fe/C, Co/C, and FeCo/C samples, respectively. The magneto-sensitive materials have proven to be effective sorbents, which can be used for contaminant concentrations from aqueous solutions.

Keywords: sawdust, activated carbon, carbon-metal composite, magneto-sensitive sorbent.

Received: 16 March 2021/ Revised final: 16 May 2021/ Accepted: 20 May 2021

Introduction

Particleboard and plywood are wood-based composite materials used for the production of furniture, construction and finishing works, etc. A significant part of worldwide production of wood composites (nearly 75 million m³ in Europe) corresponds to the wood-based panel production, 50% of which (37.8 million m³) belong to particleboard manufacturing [1]. They are manufactured by mixing chopped wood waste, shavings, and sawdust with synthetic resin binders. A significant part of the binders consists of various formaldehyde resins (e.g. urea-formaldehyde, melamine-urea-formaldehyde, melamine-formaldehyde, phenol-formaldehyde, phenol-urea-formaldehyde, resorcinol-phenol-formaldehyde resin, isocyanate resins, etc.) [2]; the exact constituents of the boards are varied from product to product. During machining of chipboard and plywood, for the production of

finished goods, a significant amount of waste is generated [1]. Solving the problem of the disposal of large-tonnage industrial wastes is one of the urgent tasks of rational nature management. To reduce the negative impact of these wastes on the environment by recycling, these composite materials could be used for the production of low-cost carbons supporting a concept of bio-resources.

The wood composites industry is a potential supplier of precursors for the production of carbon adsorbents because of high content of carbonaceous materials including both polymer mixtures of natural origin (lignocellulose from any inferior wood, both coniferous and hardwood species) and synthetic origin (resins, etc.). Nowadays many researchers use pyrolysis in an inert atmosphere of various raw biomaterials (e.g., brewers spent grain, wheat straw, grass, walnut shells, energetic willow, olive and peach

stones) in a different reactor systems as a promising approach of carbon adsorbents production due to a significant reduction of volatile products emission into the air [3-8]. Therefore, using wastes and by-products to produce carbons is attractive not only from an economic point of view, as it reduces waste disposal costs, but from an ecological standpoint, as well, helping to reduce the impact on the environment.

To improve the texture of the carbonaceous materials and their sorption properties, chemical or physical activation can be applied. The physicochemical activation provides developed porosity of activated carbons (AC) due to thermal pyrolysis and partial gasification (by steam, CO₂, H₂O₂) of the materials [9,10]. Furthermore, it was shown that the microwave treatment of raw biomaterials can effectively increase the porous structure of the carbon composites [11]. The porosity enhancement of chemically treated carbons is due to chemical dehydration reactions followed by thermal activation at relatively low temperatures [12,13].

Until recently, very little data has been published in the area of obtaining charcoals based on particleboard and plywood wastes. Gan, Q. *et al.* reported that chemical activation of medium density fibreboard sawdust with salts of zinc(II) and iron(II) with further thermal carbonisation process was not effective in developing a microporous structure, and the obtained carbons exhibited a very low adsorption capacity towards the dye [14]. However, according to Sainz-Diaz, C. *et al.* a highly microporous AC derived from furniture waste with a BET surface area of 855 m²/g were obtained in a batch fixed bed flaming pyrolyser [15]. Additionally, Gomes, J.A.F.L. *et al.* outlined the synthesis of high-porous AC with surface areas of 926 -1032 m²/g from medium-density fibreboard and particleboard using physical activation with CO₂ and chemical activation with K₂CO₃ [16]. The scattering of actual results indicates insufficient coverage of this issue. It is also worth noting that the benefit of the proposed method includes the carbonization and activation processes that can occur in one-step route, therefore significantly saving the heat energy during the synthesis. This is provided by a vertical structure of a reactor, where the atmosphere in the reaction zone contains not only argon but also the volatile products of pyrolysis. Furthermore, the developed method does not require pre-drying and dehydration of raw biomass or additional washing of AC in order to

eliminate the excess of chemicals that did not react with the material after activation.

Many methods have been developed to remove dyes from liquids, including sorption, chemical coagulation, photodegradation, biodegradation, *etc.* However, it is known that the dye sorption onto porous carbons is the most effective purification method because of large specific surface area, pore volume, chemical inertness, and good mechanical stability of carbons. Upon wastewater treatment, the carbon adsorbents are used for purification, decolorization and removal of toxic organics and heavy metal ions [17-19]. However, small particle sizes of AC cause some difficulties in the separation of spent sorbents. To improve the application characteristics of carbon adsorbents, these could be modified to obtain magnetic properties. The magnetic separation technology is receiving increasing attention because of significant simplification of the separation process of spent adsorbent particles under a weak magnetic field. Therefore, another advantage of the reported work is the ease combination of raw biomaterials with magnetic phase precursors that provide the possibility of magnetic separation of as-prepared carbon sorbents. Recently, a series of magnetic carbon composite materials have been synthesized using carbonization of metal-doped agricultural wastes and metal-polymer mixtures [20-24].

The aim of this work is the development of a new and effective approach in the production of porous magneto-sensitive carbon-inorganic composites *via* pyrolysis in argon atmosphere of chemically-activated blends of particleboard and plywood sawdust with such inorganic compounds as cobalt(II) or iron(III) chlorides separately, and their binary mixture, as well as to study their structural, textural, and adsorption properties.

Experimental

Materials

Wood sawdust (particleboard and plywood) with the size of 0.5-2.0 mm were obtained from a local factory producing furniture. Iron(III) chloride hexahydrate (≥97%) and cobalt(II) chloride hexahydrate (≥97%) were purchased from Chimlaborreactive (Ukraine) and methylene blue from Sigma-Aldrich (Germany).

Preparation of the composites

Iron(III) chloride hexahydrate and cobalt(II) chloride hexahydrate were used as precursors of a magnetic phase in the carbon/metal composites.

A general procedure of the composites' synthesis. Sawdust (fraction 0.5-2.0 mm) and metal chlorides were weighed in a glass cup, and then distilled water was added, mixed, closed with a lid and held for two days at room temperature. For the binary system Fe/Co, the molar ratio of the metals was 2:1 (Table 1). The swollen sawdust samples were placed into porcelain evaporation cups and dried at 150°C for 4 h. The resulting products of dark green (Co) and black (Fe, FeCo) colours were pyrolyzed in a vertical quartz reactor in an argon flow up to 800°C at a heating rate of 10°C/min and kept at the maximum temperature for 2 h [25]. The argon flow rate was 100 mL/min. Further cooling to room temperature was carried out in the argon flow. The composites were labelled as Co/C, Fe/C, and FeCo/C. Pyrolysis of the sawdust up to 800°C under the argon flow yields black solids with individual sawdust flakes maintaining their shape but shrinking slightly.

Characterization methods

Powder X-ray diffraction (XRD) patterns were recorded at $2\theta = 10-90^\circ$ using a DRON UMI diffractometer (Burevestnik, Saint Petersburg, Russia) with $\text{CoK}\alpha$ radiation ($\lambda = 0.17903$ nm) and a graphitic monochromator in a reflected beam. The phase composition was determined using the XRD database PDF-2. The average sizes of crystallites were calculated from the full width at half maxima of the corresponding XRD peaks by using the Scherrer equation [26]. Semi-quantitative phase analysis was performed using the Match! program.

The thermal properties as well as carbon and metal contents in the carbons were studied using the Q-1500 D derivatograph (MOM, Hungary) equipped with a computerized measurement registration system. Samples (120-125 mg) were heated in a ceramic crucible at a rate of 10°C/min in a static air atmosphere using aluminium oxide as a reference substance. The measurements were carried out at 18-1000°C in the air atmosphere.

The content of metals was estimated according to the thermogravimetric data using Eq.(1) [27].

$$m = \frac{N \cdot A \cdot n}{M} \quad (1)$$

where, m – the metal content, %;

N – the change in the weight (residue) of the sample according to TG data, %;

A – the atomic weight of the metal;

n – the number of metal atoms in the oxide formula;

M – the molecular weight of the oxide.

The carbon content was determined by subtracting the metal content and physically adsorbed water from the mass of the sample. The content of water was evaluated by mass losses on the TG curves upon heating to 150°C.

To estimate the textural characteristics, low-temperature (77.4 K) nitrogen *adsorption-desorption isotherms* were recorded using a Micromeritics ASAP 2405N adsorption analyzer. The specific surface area (S_{BET}) was calculated according to the standard BET method [28]. The total pore volume (V_p) was evaluated from the nitrogen adsorption at $p/p_0 = 0.98-0.99$ (p and p_0 denote the equilibrium and saturation pressure of nitrogen at 77.4 K, respectively). The nitrogen desorption data were used to compute the pore size distributions (*PSD*) with the modified Nguyen-Do method [29] (*PSD*, differential $f_v \sim dV_p/dR$ and $f_s \sim dS/dR$) using a model of slit-shaped pores in carbons [30,31] because the metal phase is masked by carbon in the core-shell particles. The differential *PSD* with respect to pore volume $f_v(R) \sim dV_p/dR$, $\int f_v(R)dR \sim V_p$, were recalculated as incremental *PSD* (*IPSD*, $\sum \Phi_{v,si}(R) = V_p$). The $f_v(R)$ and $f_s(R)$ functions were also used to calculate contributions of micropores (V_{micro} and S_{micro} at $R \leq 1$ nm), mesopores (V_{meso} and S_{meso} at $1 \text{ nm} < R < 25$ nm) and macropores (V_{macro} and S_{macro} at $R > 25$ nm) to the total pore volume and specific surface area.

Table 1

The ratio of components used for the preparation of the composites and the yield of the materials after pyrolysis.

Sample	Sawdust, g	H ₂ O, g	FeCl ₃ ·6H ₂ O, g	CoCl ₂ ·6H ₂ O, g	Sawdust/Metal	The yield after pyrolysis, %
Co/C	10.0	35.0	–	10.0	4.04	43.0
Fe/C	10.0	35.6	12.3	–	4.00	38.0
FeCo/C	10.0	35.5	8.2	3.0	4.10	38.2
Reference C	5.0	–	–	–	–	24.2

Unmodified sawdust carbon was used as reference C.

The morphology of carbonized composites was characterized using a JSM-6700F (GEOL) field emission scanning electron microscope.

Magnetic properties of the samples were measured by means of a SQUID magnetometer. The Magnetic Property Measuring System was used, model MPMS-XL-5 (Quantum Design, USA) equipped with 5 T superconducting magnet.

The methylene blue (MB) adsorption by carbons in series of experiments was performed at the range of 0.01-0.7 mmol/L concentrations. The sample (0.05 g) was contacted with 25 mL of a dye solution. The suspensions were shaken in an Innova 40 (New Brunswick Scientific) incubator at 110 rpm, and 25°C for 24 h. Then the equilibrium concentration of MB was determined using the spectrophotometric measurements (Cary 4000, Varian, λ_{max} = 664 nm).

The adsorption capacity q_e (mg/g) was calculated using Eq.(2).

$$q_e = V(C_o - C_e)/m \quad (2)$$

where, C_o – initial concentration of MB, mg/L;
 C_e – residual (equilibrium) concentration, mg/L;
 m – mass of adsorbent, g;
 V – volume of MB solution, L.

The potentiometric titration method was used to determine the value of surface charge density, as well as the pH_{pzc} (point of zero charge) at which the numbers of positively and negatively charged surface groups are the same. The surface charge density was calculated from the difference of the amounts of added acid or base to obtain the same pH value of suspension as for the background electrolyte. The Fe/C, FeCo/C, Co/C, or C samples were added into a 0.001 mol/L NaCl solution in a 50 mL thermostated Teflon vessel. The measurements were performed in the suspension with the same solid content, to keep the identical conditions of the experiments in the vessel at 25°C. To eliminate the influence of CO₂, the measurements were conducted in the nitrogen atmosphere. The pH values were measured using a set of glass REF 451 and calomel pHG201-8 electrodes with the Radiometer assembly.

Results and discussion

Characterization of the composites

The XRD data for the carbonized systems with a metal salt used for impregnation show the formation of several crystalline metal-containing

phases (Figure 1 and Table 2). The formation of a carbon phase with an interplanar distance of 0.338 nm of (002) reflection in the iron-containing sample is observed. A sharp and narrow peak at $2\theta = 30.58^\circ$ in the Fe/C sample indicates a quite high graphitization degree of carbon coating with the average size of crystallites of 11 nm. In the Co/C and FeCo/C samples, an amorphous phase of carbon is observed. The peaks observed at $2\theta = 45-63^\circ$ in the XRD pattern of cobalt-containing composite match with the (100), (101) and (111), (200) crystalline planes of the face centered hexagonal (ICDD no. 5-727) and cubic (ICDD no. 15-806) structures of Co, respectively. Carbonization of the sample impregnated with the salts of two metals leads to the formation of a phase of solid solution of cobalt in the crystal lattice of iron, as indicated by a shift in the reflections of iron toward larger angles (Figure 1). Cementite (Fe₃C), which gives the greatest contribution to the phase composition of Fe/C, is absent in the FeCo/C sample.

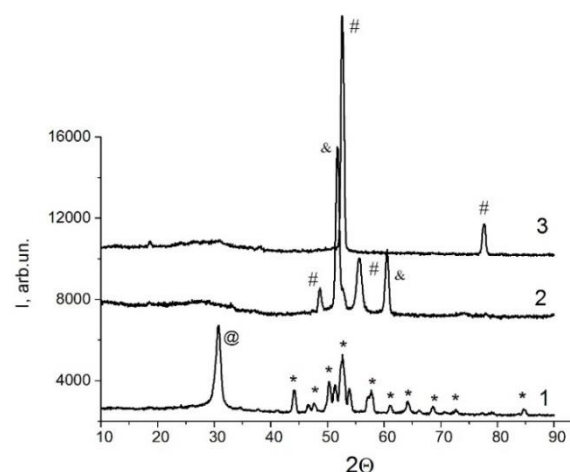


Figure 1. XRD patterns of the composites: Fe/C (1), Co/C (2) and– FeCo/C (3). ((@)– graphite phase; (*)– cementite (Fe₃C); (#)– cubic structures; (&)- hexagonal structures)

Table 2

Phase composition and crystallite size of the samples.

Sample	Phase composition	Crystalline phases, %	D_{cr} , nm
Fe/C	C _{graphite}	35	11
	Fe ₃ C	60	22
	Fe	5	20
Co/C	Co _{cub}	64	22
	Co _{hex}	36	23
FeCo/C	Fe _{cub}	100	25

The morphology of the materials was characterized using SEM and the images are shown in Figure 2. A certain microstructure of the biomass used has been retained during carbonization giving an open framework of aligned straight fibrils of different sizes with an array of pores of about 3-5 μm . Figures 2(c) and (f) show that their cross section has a honeycomb-like structure. However, it is difficult to compare the diameter of these fibrils in different samples taking into account the composition and structure of the waste precursors, especially when different methods were used to produce the wood materials (particleboard and chipboard).

The SEM images show that a surface of the unmodified sample includes porous smooth fibrils with plenty of interconnected pores, but the presence of structures of porous wood is insignificant (Figure 2(a)). The images of metal-containing composites show that the morphology of the materials changed after the modification and pyrolysis. The formation of composites with a rough morphology and diversified types of protuberances, as well as with cracks and cavities and less uniformity is observed (Figure 2(b)-(i)). The appearance of

larger pores and cracks can be attributed to the decomposition of fibrous structures during the process. Apart from that, the highly disperse metal nanoparticles in the carbon matrix and large aggregates of irregular shapes at the outer surfaces of the granules are registered (Figure 2(c), (e), (g), and (h)). Furthermore, modification by metals caused the formation of a complex corrugated surface with multiple pores of diameters ranging between 500 and 1000 nm (Figure 2(d) and (g)); however, the pores were not filled and the porosity was maintained.

It is well known that graphitized carbons with a high graphitization degree are more stable against air oxidation. Therefore, the TG-DTG analysis was used to study the air-resistance of the prepared carbons. Figure 3 presents the TG and DTG curves for metal-containing carbons and reference carbon. There are two main mass losses on the TG curves of the reference sample. The first one is due to evaporation of physically adsorbed water (< 200°C) and then carbon combustion (> 250°C) took place with the removal of volatile products (DTG_{max} ≈ 580°C).

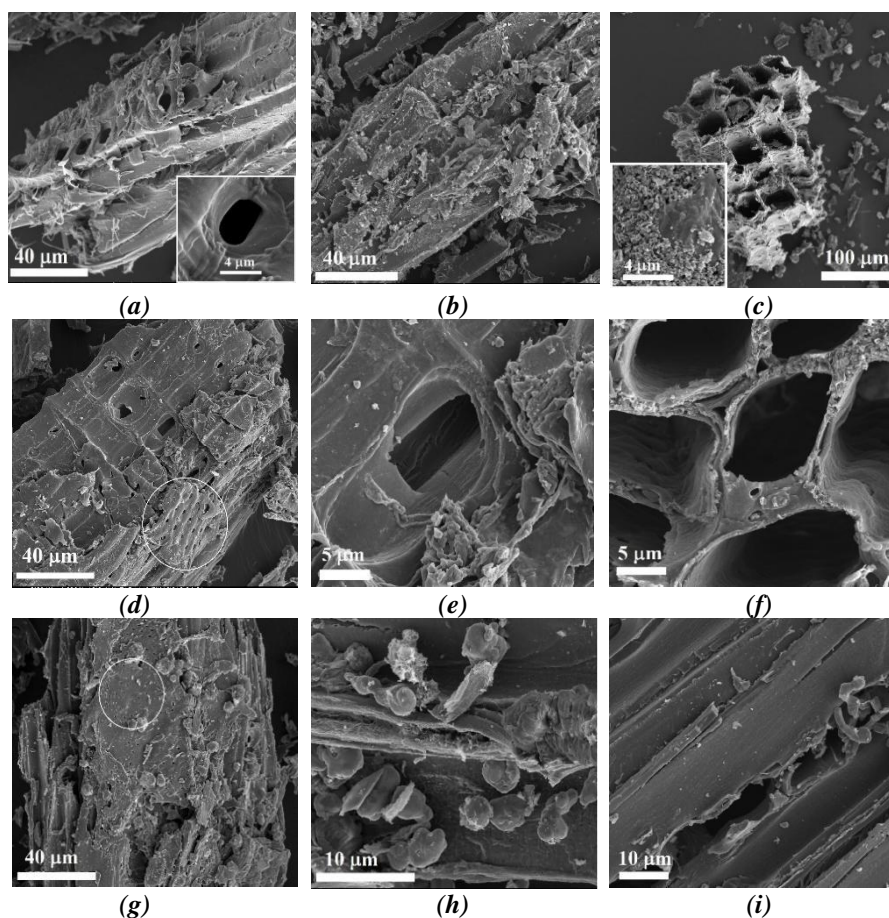


Figure 2. SEM images of the samples: reference C (a); Co/C (b), (c); Fe/C (d)-(f); FeCo/C (g-i).

From the DTG curves of the as-prepared metal-containing composites (Figure 3), several distinct peaks in different temperature ranges can be seen, indicating a multistage character of the processes in the carbons. During thermooxidative destruction of porous carbon-containing composites a series of chemical reactions took place. The TG and DTG curves can be divided into several sections vs. temperature: (i) weight loss during heating from room temperature to 200°C corresponding to desorption of physically adsorbed water (DTG_{max} ≈ 110°C); (ii) complex thermooxidative process after treatment at 200°C. The curves of the mass changes show the result of two opposite processes, such as mass increasing due to oxidation of metal phase because of reaction with oxygen from the air, and mass reduction during carbon burn-off and CO₂ removal. This is especially evident in the Fe/C sample (Figure 3); (iii) weight decrease upon heating to ~ 850–980°C indicating the final oxidation and formation of metal oxides. Taking into account that the TG curves of the metal-doped composites bend at about 100°C lower compared to the reference, metal modification caused deterioration of thermal

resistance for carbons due to the catalytic effects of metallic nanoparticles, which became accessible for oxygen molecules. The different thermal resistances of the carbon phase in different composites are due to the difference in the morphology of the carbon phase. The greater the density of aggregates, the higher is the temperature of complete oxidation of the particles. This correlates with the reduced value of the specific surface area and is confirmed by SEM images.

The content of iron and cobalt in the samples was calculated based on the TG analysis. Heating of the metal-carbon nanocomposites up to 1000°C in air is accompanied by complete oxidation of carbon to CO₂ and of metals to oxides. Considering the initial weight of the samples and the residual weight after heating up to 1000°C, the contents of metallic iron and cobalt could be estimated (Table 3) using Eq.(1). The formation of two types of oxides Co₃O₄ and Fe₂O₃ was considered, because those were the main phases according to XRD data after the thermal-oxidative destruction of the corresponding salts in air [34].

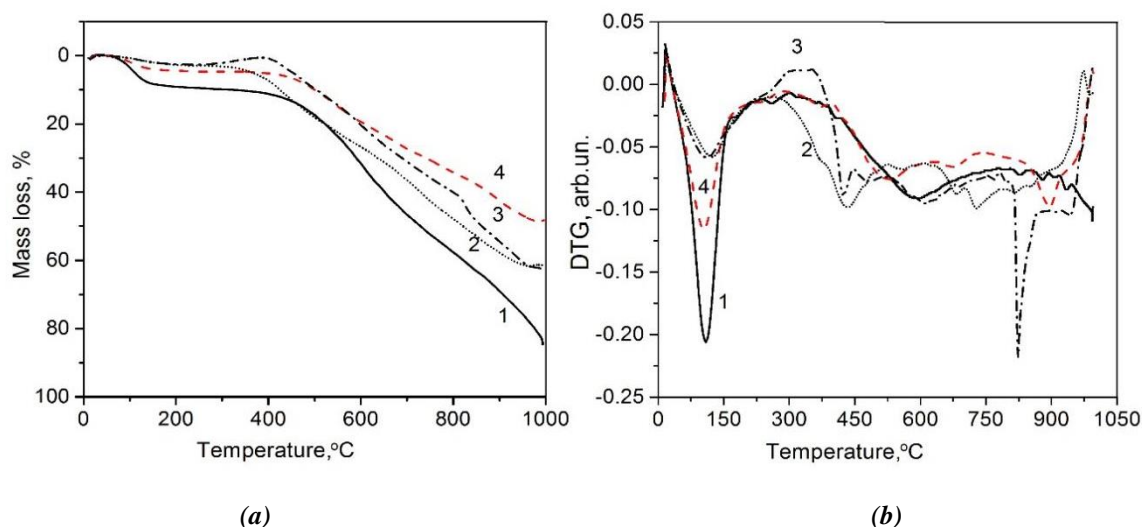


Figure 3. TG (a) and DTG (b) curves of the samples: reference C (1); FeCo/C (2); Fe/C (3); Co/C (4).

Table 3

Mass residue, carbon and metal content determined by TG measurement.

Sample	Carbon content ¹ , %	Metal content ² , %	Mass residue ³ , %
Fe/C	74.9	25.1	37.6
Co/C	60.1	39.9	51.5
FeCo/C	73.0	18.8 (Fe); 8.2 (Co)	38.7
reference C	91.7	-	2.2

¹ Carbon content in the samples without adsorbed water (at 150°C on the TG curve);

² Metal content in the composites with correction for ash content in carbon and adsorbed water;

³ Mass residue according to the TG data, after cooling the sample to room temperature together with the furnace of the derivatograph;

The source of errors (less than 5%) is the ash content in sawdust and CoO impurity in the FeCo/C sample.

Figure 4(a) presents the nitrogen adsorption/desorption isotherms measured at 77.4 K for the composites. The composites exhibited adsorption isotherms of type I and IV according to IUPAC classification, corresponding to the materials with micro- and mesoporosity [33]. The type H3 of hysteresis loops indicates the appearance of pores of slit-like shape and capillary of non-parallel walls, typical for carbon materials. The effect of the filler on pore characteristics of composites during pyrolysis is significant. The larger adsorption at low p/p_0 of the Co/C and FeCo/C samples confirm the presence of micropores. Meanwhile, the Fe/C sample exhibited a wide hysteresis loop in the relative pressure range of 0.45-1 indicating the presence of mesoporosity (Figure 4(a)). Additionally, high increase of adsorption for relative pressures over 0.8 corresponds to adsorption in macropores. The isotherm for the reference (C sample) is not presented due to very low adsorption. The Co-containing samples show an intensive PSD peak of micropores, but the Fe/C sample shows larger contribution of mesoporous with several peaks (Figure 4(b)). Moreover, the capillary condensation

effect becomes greater in the line Co/C < FeCo/C < Fe/C that indicates the mesopores broadening.

The specific surface area of the Co/C and FeCo/C samples is 328 and 391 m^2/g , respectively, (Table 4) and it is much larger than S_{BET} of the reference C sample ($S_{BET} = 4 m^2/g$). A smaller value for the Fe/C sample (58 m^2/g) is due to the carbide phase formation. A decrease in the specific surface area and pore volume (V_p) with simultaneous increase in the mesoporosity is due to the strong oxidation effect of the metals that leads to destruction of the pore walls with enhanced effect of burn-off [32].

Adsorption capacity for methylene blue

Magneto-sensitive porous carbon adsorbents are highly attractive for many applications associated with liquid-phase processes. In this study, MB was chosen as a model pollutant for adsorption experiments. The equilibrium MB adsorption was studied at natural pH in an aqueous solution at 25°C. The experiments show that the adsorption capacity decreases as follows 31 > 28 > 2.8 mg/g in the line Fe/C > FeCo/C > Co/C, respectively.

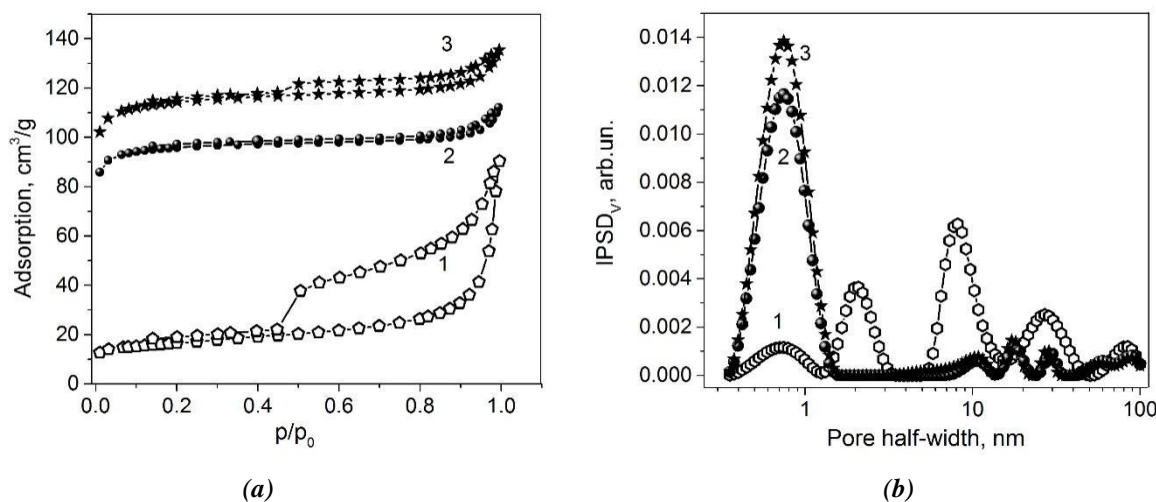


Figure 4. Textural characteristics of the Fe/C (1); Co/C (2); FeCo/C (3) composites: low-temperature nitrogen adsorption/desorption isotherms (a) pore size distribution curves (b).

Table 4

Structural characteristics of the composites.										
Sample	S_{BET} , m^2/g	S_{micro} , m^2/g	S_{meso} , m^2/g	S_{macro} , m^2/g	V_p , cm^3/g	V_{micro} , cm^3/g	V_{meso} , cm^3/g	V_{macro} , cm^3/g	V_{micro}/V_p	V_{meso}/V_p
reference C	4	-	-	-	-	-	-	-	-	-
Fe/C	58	27	30	0.7	0.13	0.01	0.10	0.02	0.1	0.74
Co/C	328	311	17	0.3	0.17	0.14	0.02	0.01	0.82	0.12
FeCo/C	391	369	22	0.3	0.21	0.17	0.03	0.01	0.81	0.15

It does not show a direct proportionality between the specific surface area and adsorbed MB quantities. It is clear that the mesopore volume is the main factor determining the MB adsorption. Fe/C composite exhibited the highest adsorption capacity for MB removal from water (31 mg/g) due to its large mesoporosity (77% of the total pore volume). In the case of Co/C and FeCo/C, the contribution of micropores was much greater (82% and 81% of the total pore volume, respectively) and therefore the adsorption value of the dye was reduced. MB molecules are too large to be adsorbed in narrow and long micropores. The adsorption capacity of the reference composite was close to zero because of very low porosity and specific surface area (Figure 5).

Additionally, there is a correlation between the dye exchange capacity and surface charge density of the adsorbents [35]. It was shown, that the process of adsorption of organic compounds on AC occurs mainly as a result of two main types of factors: the dispersion interactions (between the aromatic rings of adsorbate molecules and graphene layers of AC), and electrostatic interactions. Figure 6 shows the surface charge density of composites as a function of pH. At pH of 1-3, the electric charge of carbons is not only positive but also negative. The pH_{pzc} for the samples are 5.2, 7.0, and 9.4 for Fe/C, FeCo/C, and Co/C, respectively. It is expected that adsorption of a cationic dye MB will occur better at high pH values. The experimental study has confirmed this assumption. The Fe/C sample has a higher efficiency of sorption due to the pH matching of its pH_{pzc} with used experimental pH value, whereas the FeCo/C and Co/C samples need significantly higher pH values for better adsorption of MB. Thus, not only the textural characteristics of the carbon composites but also

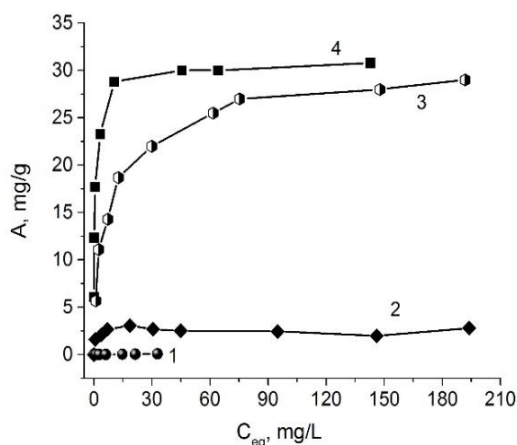


Figure 5. Equilibrium adsorption isotherms of MB onto the composites: reference C (1); Co/C (2); FeCo/C (3); Fe/C (4).

the chemical structure of their surface (e.g. the presence and amounts of various O-containing surface sites) can affect the MB adsorption.

Magnetic properties of nanocomposites

The magnetic properties of the materials were evaluated using magnetic hysteresis curves (Figure 7). According to the XRD data (Figure 1, Table 2), salts in the Co/C and FeCo/C samples were completely reduced to metallic state with the formation of face-centered cubic and hexagonal Co phases in the Co/C sample and only cubic Fe phase in the FeCo/C sample. Whereas the phase state of the nanocomposite based on Fe/C is quite complex and can be described by different sets of carbides and the formation of significant number of graphite-like structures.

The saturation magnetization values (M_s , determined at 5 T) are much lower than those of the corresponding iron and cobalt bulk metal values [36,37]. The highest magnetization saturation was observed for Co/C composite that corresponds to ca. 1/3 of bulk metal value. This composite contains the highest fraction of ferromagnetic metal particles. The higher magnetization of the FeCo/C nanocomposite compared to that of Fe/C could be attributed to the effect of cobalt. For Fe/C sample, the reducing of the magnetization can be due to the formation of the FeC_3 phase. Thus, the low saturation magnetization of the samples may be attributed to the presence of different fractions of magnetic and non-magnetic phases. Additionally, it may be related to weak interaction of the magnetic domains because of the high amount of diamagnetic graphite in the samples. The sizes of nanoparticles may affect the value of the coercive field due to size influence of the magnetization of nanoparticles.

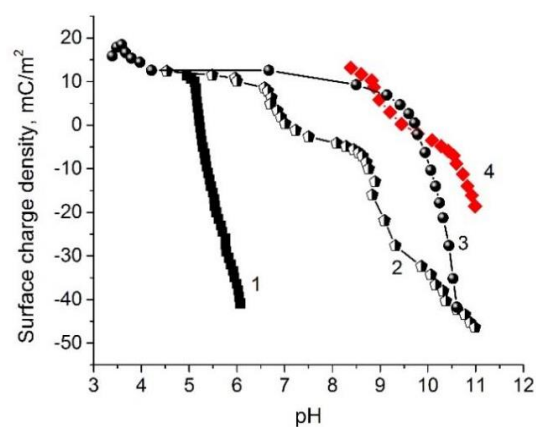


Figure 6. The surface charge density as a function of pH for composites, suspended in 0.001 mol/L NaCl solution: Fe/C (1); FeCo/C (2); reference C (3); Co/C (4).

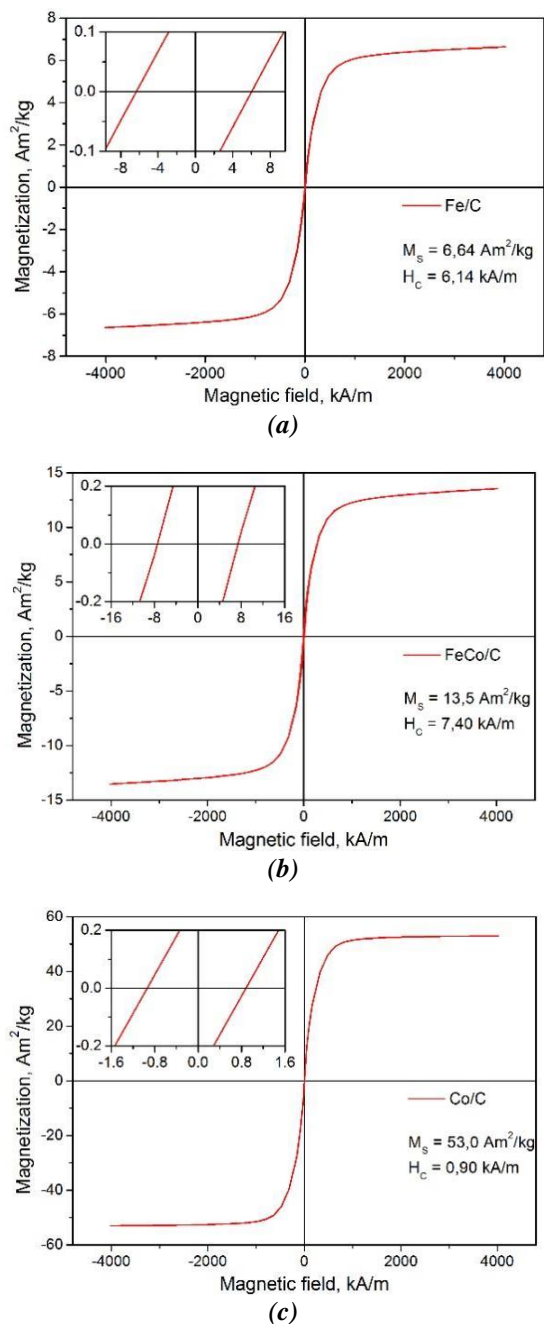


Figure 7. Magnetic hysteresis loops of the composites: Fe/C (a); FeCo/C (b); Co/C (c).

Hereby, prepared samples exhibit typically soft magnetic features and can be easily attracted by a magnet after adsorption that provides an efficient way to separate spent magnetic composites from liquids. Furthermore, magnetically separable porous carbon composites are highly attractive options for many applications associated with liquid-phase processes. The presented study represents a starting point for future researches on the recycling and reuse of sawdust wastes and related materials.

Conclusions

An effective approach in production of adsorbents with developed porous structure and appropriate magnetic susceptibility was reported in this study. The composition-structure-property relationship was identified in the process of thermal transformation of modified raw materials.

It was shown that the type of dopants had a significant effect on the morphology, porosity and magnetic properties of composites. Activation of the sawdust by iron(III) chloride promoted recovery of iron to metallic state and formation of Fe_3C and crystalline carbon. In the case of cobalt(II) chloride, the formation of metal nanoparticles of cobalt in cubic and hexagonal crystalline modifications in an amorphous carboxyl matrix took place. Activation of sawdust with the binary mixture of cobalt(II) and iron(III) chlorides led to the recovery of metals during pyrolysis with the formation of only cubic crystalline modification without the presence of crystalline carbon.

It was established that the changes in the textural/structural properties of the composites depended strongly on the dopant type. The specific surface area of composites increased in the series $\text{Fe/C} < \text{Co/C} < \text{FeCo/C}$ from 58 to 391 m^2/g , whereas the reference sample of carbonized sawdust had only 4 m^2/g . The calculated mesopore volume decreased in the series $\text{Fe/C} < \text{FeCo/C} < \text{Co/C}$ from 0.10 to 0.02 cm^3/g . Meanwhile, the mesoporosity correlated with the adsorption capacity of nanocomposites towards the cationic dye. Thus, the mesopore volume can be the decisive factor determining the methylene blue adsorption.

The saturation magnetization values of the obtained metal-carbon composites varied in the series $\text{Fe/C} < \text{FeCo/C} < \text{Co/C}$ from 6.64 to 53.0 Am^2/kg . The Fe/C sample had the lowest M_s due to the large number of non-magnetic Fe_3C component.

Thus, varying the nature of chemical activators of carbon makes it possible to regulate the sorption and magnetic properties of carbon-inorganic composites for targeted use in technological processes.

Funding

M.G. gratefully acknowledges the financial support provided by the International Visegrad Fund (Scholarship no. 51910536).

The authors are grateful to the Ministry of Education and Science of Ukraine for the support of the work (project no. M/118-2018).

References

1. UNECE/FAO Forest Products Annual Market Review, 2018-2019. <https://unece.org/forests/fpamr-2018-2019>
2. Prasittisopin, L.; Li, K. A new method of making particleboard with a formaldehyde-free soy-based adhesive. *Composites Part A: Applied Science and Manufacturing*, 2010, 41(10), pp. 1447-1453. DOI: <https://doi.org/10.1016/j.compositesa.2010.06.006>
3. Czajczyńska, D.; Anguilano, L.; Ghazal, H.; Krzyżyńska, R.; Reynolds, A.J.; Spencer, N.; Jouhara, H. Potential of pyrolysis processes in the waste management sector. *Thermal Science and Engineering Progress*, 2017, 3, pp. 171-197. DOI: <https://doi.org/10.1016/j.tsep.2017.06.003>
4. Skubiszewska-Zięba, J.; Charmas, B.; Kołtowski, M.; Oleszczuk, P. Active carbons from waste biochars: Structural and thermal properties. *Journal of Thermal Analysis and Calorimetry*, 2017, 130, pp. 15-24. DOI: <https://doi.org/10.1007/s10973-017-6143-5>
5. Kołtowski, M.; Charmas, B.; Skubiszewska-Zięba, J.; Oleszczuk, P. Effect of biochar activation by different methods on toxicity of soil contaminated by industrial activity. *Ecotoxicology and Environmental Safety*, 2017, 136, pp. 119-125. DOI: <https://doi.org/10.1016/j.ecoenv.2016.10.033>
6. Mahmood, A.S.N.; Brammer, J.G.; Hornung, A.; Steele, A.; Poulston, S. The intermediate pyrolysis and catalytic steam reforming of Brewers spent grain. *Journal of Analytical and Applied Pyrolysis*, 2013, 103, pp. 328-342. DOI: <https://doi.org/10.1016/j.jaap.2012.09.009>
7. Duman, G.; Okutucu, C.; Ucar, S.; Stahl, R.; Yanik, J. The slow and fast pyrolysis of cherry seed. *Bioresource Technology*, 2011, 102(2), pp. 1869-1878. DOI: <https://doi.org/10.1016/j.biortech.2010.07.051>
8. Ferro-Garcia, M.A.; Rivera-Utrilla, J.; Rodriguez-Gordillo, J.; Bautista-Toledo, I. Adsorption of zinc, cadmium, and copper on activated carbons obtained from agricultural by-products. *Carbon*, 1988, 26(3), pp. 363-373. DOI: [https://doi.org/10.1016/0008-6223\(88\)90228-X](https://doi.org/10.1016/0008-6223(88)90228-X)
9. Leboda, R.; Skubiszewska-Zięba, J.; Bogillo, V.I. Influence of gasification catalyzed by calcium and steam activation on the porous structure of activated carbons. *Langmuir*, 1997, 13(5), pp. 1211-1217. DOI: <https://doi.org/10.1021/la951564x>
10. Leboda, R.; Skubiszewska-Zięba, J.; Grzegorzczak, W. Effect of calcium catalyst loading procedure on the porous structure of active carbon from plum stones modified in the steam gasification process. *Carbon*, 1998, 36(4), pp. 417-425. DOI: [https://doi.org/10.1016/S0008-6223\(97\)00221-2](https://doi.org/10.1016/S0008-6223(97)00221-2)
11. Miura, M.; Kaga, H.; Sakurai, A.; Kakuchi, T.; Takahashi, K. Rapid pyrolysis of wood block by microwave heating. *Journal of Analytical and Applied Pyrolysis*, 2004, 71(1), pp. 187-199. DOI: [https://doi.org/10.1016/S0165-2370\(03\)00087-1](https://doi.org/10.1016/S0165-2370(03)00087-1)
12. Wan Isahak, W.N.R.; Hisham, M.W.M.; Yarmo, M.A. Highly porous carbon materials from biomass by chemical and carbonization method: A comparison study. *Journal of Chemistry*, 2013, 620346, pp. 1-6. DOI: <https://doi.org/10.1155/2013/620346>
13. Duca, Gh.; Ciobanu, M.; Lupascu, T.; Povar I.; Adsorption of strontium ions from aqueous solutions on nut shells activated carbons. *Chemistry Journal of Moldova*, 2018, 13(2), pp. 69-73. DOI: <https://dx.doi.org/10.19261/cjm.2018.494>
14. Gan, Q.; Allen, S.J.; Matthews, R. Activation of waste MDF sawdust charcoal and its reactive dye adsorption characteristics. *Waste management*, 2004, 24(8), pp. 841-848. DOI: <https://doi.org/10.1016/j.wasman.2004.02.010>
15. Saniz-Diaz, C.I.; Griffiths, A.J. Activated carbon from solid wastes using a pilot-scale batch flaming pyrolyser. *Fuel*, 2000, 79(15), pp. 1863-1871. DOI: [https://doi.org/10.1016/S0016-2361\(00\)00052-1](https://doi.org/10.1016/S0016-2361(00)00052-1)
16. Gomes, J.A.F.L.; Azaruja, B.C.; Mourão, P.A.M. MDF and PB activated carbons for adsorption of dyes from liquid phase. *Ciência & Tecnologia dos Materiais*, 2015, 29(1), pp. e219-e223. DOI: <https://doi.org/10.1016/j.ctmat.2016.08.001>
17. Mourid, E.; Lakraimi, M.; Khattabi, E.El; Benaziz, L.; Berraho, M. Removal of textile dye acid green 1 from wastewater by activated carbon. *Journal of Materials and Environmental Sciences*, 2017, 8(9), pp. 3121-3130. http://www.jmaterenvironsci.com/Document/vol8/vol8_N9/330-JMES-3405-Moufid.pdf
18. Kobya, M.; Demirbas, E.; Senturk, E.; Ince, M. Adsorption of heavy metal ions from aqueous solutions by activated carbon prepared from apricot stone. *Bioresource Technology*, 2005, 96(13), pp. 1518-1521. DOI: <https://doi.org/10.1016/j.biortech.2004.12.005>
19. Branton, P.; Bradley, R.H. Effects of active carbon pore size distributions on adsorption of toxic organic compounds. *Adsorption*, 2011, 17, pp. 293-301. DOI: <https://doi.org/10.1007/s10450-010-9284-4>
20. Bogatyrov, V.M.; Galaburda, M.V.; Oranska, O.I.; Borysenko, M.V.; Charmas, B.; Skubiszewska-Zięba, J.; Komar, M.A.; Voitko, I.I. Synthesis and adsorption properties of cobalt-carbon nanocomposites on the basis of sunflower seed husks. *Surface*, 2017, 9(24), pp. 145-155. (in Russian). DOI: <https://doi.org/10.15407/Surface.2017.09.145>

21. Galaburda, M.V.; Bogatyrov, V.M.; Tomaszewski, W.; Oranska, O.I.; Borysenko, M.V.; Skubiszewska-Zięba, J.; Gun'ko, V.M. Adsorption/desorption of explosives on Ni-, Co-, and NiCo-carbon composites: Application in solid phase extraction. *Colloids and Surfaces A: Physicochemical and Engineering Aspects*, 2017, 529, pp. 950-958. DOI: <https://doi.org/10.1016/j.colsurfa.2017.06.087>
22. Bogatyrov, V.M.; Galaburda, M.V.; Tomaszewski, W.; Skubiszewska-Zięba, J. Effect of the surface properties of resorcinol-formaldehyde resin/carbon nanocomposites and their carbonization products on the solid-phase extraction of explosives. *RSC Advances*, 2017, 7(12), pp. 7033-7040. DOI: <https://doi.org/10.1039/C6RA25822K>
23. Galaburda, M.V.; Bogatyrov, V.M.; Skubiszewska-Zięba, J.; Oranska, O.I.; Sternik, D.; Gun'ko, V.M. Synthesis and structural features of resorcinol-formaldehyde resin chars containing nickel nanoparticles. *Applied Surface Science*, 2016, 360, Part B, pp. 722-730. DOI: <https://doi.org/10.1016/j.apsusc.2015.11.053>
24. Galaburda, M.V.; Bogatyrov, V.M.; Oranska, O.I.; Skubiszewska-Zięba, J.; Gun'ko, V.M.; Sternik, D. Magneto-sensitive Ni/C adsorbents: synthesis, properties and applications. *Adsorption Science & Technology*, 2015, 33, pp. 523-529. DOI: <https://doi.org/10.1260/0263-6174.33.6-8.523>
25. Bogatyrov, V.M.; Galaburda, M.V.; Oranska, O.I.; Borysenko, M.V.; Vasileva, E.A.; Voitko, I.I. Synthesis and adsorption properties of magneto-sensitive nanocomposites based on Ni/C. *Surface*, 2015, 7(22), pp. 196-204. (in Russian). DOI: <https://doi.org/10.15407/Surface>
26. Jenkins, R.; Snyder, R.L. Introduction to X-ray powder diffractometry. New York: Wiley, 1996, 432 p. DOI: [10.1002/9781118520994](https://doi.org/10.1002/9781118520994)
27. Bogatyrov, V.M.; Borysenko, M.V.; Oranska, O.I.; Galaburda, M.V.; Makhno, S.M.; Gorbyk, P.P. Synthesis and properties of metal-carbon nanocomposites Ni/C, Co/C and Cu/C with high metal content. *Surface*, 2017, 9(24), pp. 136-144. (in Russian). DOI: <https://doi.org/10.15407/Surface.2017.09.136>
28. Gregg, S.J.; Sing, K.S.W. Adsorption, surface area and porosity. London: Academic Press, 1982, 303 p.
29. Gun'ko, V.M.; Do, D.D. Characterization of pore structure of carbon adsorbents using regularization procedure. *Colloids and Surfaces A: Physicochemical and Engineering Aspects*, 2001, 193(1-3), pp. 71-83. DOI: [https://doi.org/10.1016/S0927-7757\(01\)00685-9](https://doi.org/10.1016/S0927-7757(01)00685-9)
30. Gun'ko, V.M. Composite materials: textural characteristics. *Applied Surface Science*, 2014, 307, pp. 444-454. DOI: <https://doi.org/10.1016/j.apsusc.2014.04.055>
31. Gun'ko, V.M.; Mikhalovsky, S.V. Evaluation of slitlike porosity of carbon adsorbents. *Carbon*, 2004, 42(4), pp. 843-849. DOI: <https://doi.org/10.1016/j.carbon.2004.01.059>
32. Galaburda, M.; Bogatyrov, V.; Oranska, O.; Gun'ko, V.; Skubiszewska-Zięba, J.; Urubkov, I. Synthesis and characterization of carbon composites containing Fe, Co, Ni nanoparticles. *Journal of Thermal Analysis and Calorimetry*, 2015, 122, pp. 553-561. DOI: <https://doi.org/10.1007/s10973-015-4819-2>
33. Rouquerol, J.; Avnir, D.; Fairbridge, C.W.; Everett, D.H.; Haynes, J.H.; Pernicone, N.; Ramsay, J.D.F.; Sing, K.S.W.; Unger, K.K. IUPAC Recommendation for the characterization of porous solids. *Pure and Applied Chemistry*, 1994, 66(8), pp. 1739-1758. DOI: <https://doi.org/10.1351/pac199466081739>
34. Moreno-Castilla, C.; Carrasco-Marín, F.; Maldonado-Hodar, F.J.; Rivera-Utrilla, J. Effects of non-oxidant and oxidant acid treatments on the surface properties of an activated carbon with very low ash content. *Carbon*, 1998, 36(1-2), pp. 145-151. DOI: [https://doi.org/10.1016/S0008-6223\(97\)00171-1](https://doi.org/10.1016/S0008-6223(97)00171-1)
35. Derylo-Marczewska, A.; Marczewski, A.W.; Winter, Sz.; Sternik, D. Studies of adsorption equilibria and kinetics in the systems: Aqueous solution of dyes-mesoporous carbons. *Applied Surface Science*, 2010, 256(17), pp. 5164-5170. DOI: <https://doi.org/10.1016/j.apsusc.2009.12.085>
36. Zhu, G.X.; Wei, X.W.; Xia, C.J.; Ye, Y. Solution route to single crystalline dendritic cobalt nanostructures coated with carbon shells. *Carbon*, 2007, 45(6), pp. 1160-1166. DOI: <https://doi.org/10.1016/j.carbon.2007.02.028>
37. Park, J.B.; Jeong, S.H.; Jeong, M.S.; Kim, J.Y.; Cho, B.K. Synthesis of carbon-encapsulated magnetic nanoparticles by pulsed laser irradiation of solution. *Carbon*, 2008, 46(11), pp. 1369-1377. DOI: <https://doi.org/10.1016/j.carbon.2008.05.011>